Report

Current Biology

Extreme Compartmentalization in a *Drosophila* Amacrine Cell

Highlights

- Individual terminals of fly amacrine cell CT1 exhibit strong compartmentalization
- Each CT1 terminal has a distinct visual receptive field
- Biophysical modeling links morphology to signal compartmentalization
- CT1 can thus support local motion detection

Authors

Matthias Meier, Alexander Borst

Correspondence

mmeier@neuro.mpg.de (M.M.), aborst@neuro.mpg.de (A.B.)

In Brief

Meier and Borst characterize a large-field amacrine cell in the fly optic lobe and show that this single cell acts as hundreds of parallel functional units. Using calcium imaging and compartmental modeling, the authors demonstrate extreme electrical isolation of signals in individual terminals at the biophysical limit of neural computation.

Meier & Borst, 2019, Current Biology *29*, 1545–1550
May 6, 2019
https://doi.org/10.1016/j.cub.2019.03.070

CellPress

Current Biology
Report

Extreme Compartmentalization in a *Drosophila* Amacrine Cell

Matthias Meier[1,2,*] and Alexander Borst[1,*]
[1]Max Planck Institute of Neurobiology, 82152 Martinsried, Germany
[2]Lead Contact
*Correspondence: mmeier@neuro.mpg.de (M.M.), aborst@neuro.mpg.de (A.B.)
https://doi.org/10.1016/j.cub.2019.03.070

SUMMARY

A neuron is conventionally regarded as a single processing unit. It receives input from one or several presynaptic cells, transforms these signals, and transmits one output signal to its postsynaptic partners. Exceptions exist: amacrine cells in the mammalian retina [1–3] or interneurons in the locust mesothoracic ganglion [4] are thought to represent many electrically isolated microcircuits within one neuron. An extreme case of such an amacrine cell has recently been described in the *Drosophila* visual system. This cell, called CT1, reaches into two neuropils of the optic lobe, where it visits each of 700 repetitive columns, thereby covering the whole visual field [5, 6]. Due to its unusual morphology, CT1 has been suspected to perform local computations [6, 7], but this has never been proven. Using 2-photon calcium imaging and visual stimulation, we find highly compartmentalized retinotopic response properties in neighboring terminals of CT1, with each terminal acting as an independent functional unit. Model simulations demonstrate that this extreme case of compartmentalization is at the biophysical limit of neural computation.

RESULTS AND DISCUSSION

The visual system of the fruit fly comprises the eye with about 700 facets and the optic lobe. The latter consists of four layers of retinotopically organized neuropils called lamina, medulla, lobula, and lobula plate. Within each column of both medulla and lobula, CT1 receives input from a number of local interneurons and makes output synapses onto elementary motion-detecting T4 and T5 cells [7]. T4 cells are sensitive to bright moving edges and have their dendrites in the most proximal layer of the medulla. T5 cells respond preferentially to dark moving edges and extend their dendrites into the posterior layer of the lobula. Both come in four subtypes, one for each of the four cardinal directions of visual motion [8]. For each subtype, the synapses of CT1 are located precisely on the null direction side of T4 and T5 dendrites [7]. Therefore, CT1 has been speculated to be of functional relevance for creating direction selectivity within T4 and T5, in particular because it receives excitatory, cholinergic input and releases the typically inhibitory neurotransmitter GABA, which may introduce a sign inversion [6]. To support motion detection, however, the columnar processes of CT1 must act as spatially independent, local processing units. Curiously, these structures are connected to major branches via ultrathin, 0.1-μm-wide processes that form loops and, thus, are about 10 times longer than needed to bridge the distance between neighboring columns (Figure 1D) [7].

To measure the receptive fields of individual processes in CT1, we used calcium levels—as a proxy for neural activity [9, 10]—recorded under a 2-photon microscope during visual stimulation with a white-noise bar pattern [11]. By correlating the fluorescence signal of a given neural process with the stimulus intensity at each location in space and time, a spatiotemporal receptive field was obtained. As shown in a representative experiment (Figure 2A), each compartment of CT1 has its own confined receptive field with a small half-width, comparable to the size of the interommatidial angle of the fly eye. Furthermore, receptive field centers are displaced with respect to neighboring compartments. Processes within the medulla are ON-sensitive and the ones in the lobula are OFF-sensitive (Figure 2B), just like their postsynaptic partner cells, T4 and T5. To assess the spatiotemporal response properties more closely, we took such measurements from many compartments of CT1 cells and averaged their receptive fields after alignment to their center. The spatial profile of the processes in the medulla reveal an ON-center with a full-width at half maximum of 9.1° and temporal band-pass characteristics (Figure 2C). The spatial profile in the lobula reveals an OFF-center with a half-width of 7.2° (Figure 2D). Receptive field sizes determined at different locations in visual space were rather similar (Figure S1). To test the selectivity of the compartments to contrast polarity as well as their potential direction selectivity, we used bright and dark edges moving in 12 directions (Figures 2C and 2D, insets). CT1 compartments respond selectively to either moving ON (medulla) or OFF (lobula) edges, irrespective of the direction of motion.

This extreme compartmentalization requires strong electrical isolation of neural processes within neighboring columns. Given the minute absolute distances in the fruit fly brain, we wondered whether this is at all possible. We therefore built a realistic, electrically passive compartmental model of CT1, based on electron microscopy reconstructions [7]. It consists of 11 terminals in the medulla that are connected via thin, looping branches to several thicker parental branches (Figures 1D and 3A). Using biophysically plausible membrane parameters [12] and direct current (DC) injections into one columnar compartment at a time

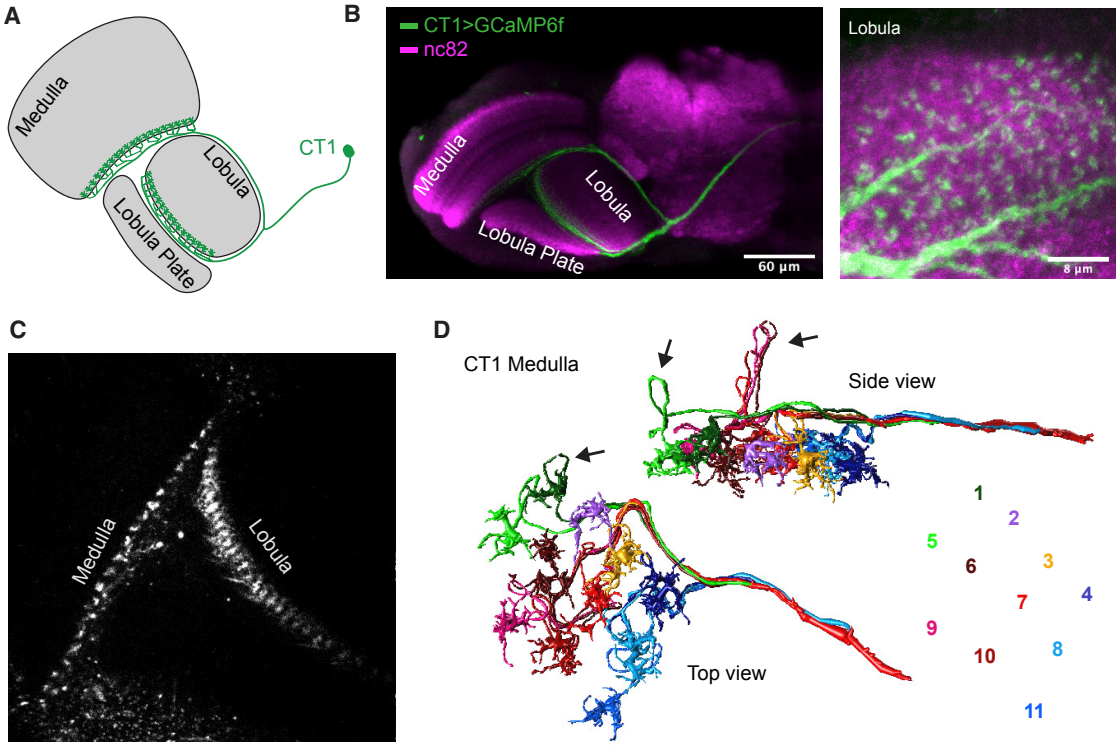

Figure 1. Anatomy of CT1

(A) Schematic drawing of CT1 innervating all columns in both medulla and lobula.

(B) Fluorescent images of CT1. (Left) Overview of CT1 ramifications (GCaMP expression green) in one hemisphere of the fly brain (magenta: nc82 background staining) is shown. (Right) Columnar branching pattern of CT1 in the lobula is shown.

(C) 2-photon image of the fluorescence signal of CT1 as seen under the microscope.

(D) 3D reconstruction of 11 CT1 terminals in the medulla (top view and side view of the same model; data from [7]). Similar colors (green, red, and blue) correspond to similar parent branches. Arrows highlight loops in the neural processes. The column identity of each CT1 terminal is indicated at the bottom right.

(Figure 3A, gray electrodes), we investigated the distribution of membrane voltage across the whole model cell. Irrespective of the stimulated column, the voltage drops steeply to a level of around 20% in all remaining compartments, indicating strong electrical isolation of each CT1 terminal from its neighbors. As a control, we calculated the same current injection into the tip of the thick main branch (Figure 3A, lower right). As expected, the voltage spreads more uniformly under these conditions and drops to only about 50% of the peak voltage [13]. Next, we examined how the compartmentalization of the model cell depends on the choice of parameters for the axial (R_a) and transmembrane (R_m) resistance. To this end, we simulated current injections into one compartment and measured the average relative membrane potential in all other terminals while varying the values for R_a and R_m (Figure 3B). We found that the model only retains a high degree of compartmentalization if R_a is rather high or if R_m is low. We then wondered how this translates into receptive field properties of an isolated CT1 terminal, as determined in our imaging experiments. To test this, we simulated synaptic input into one compartment, assuming three Gaussian input signals of 7° half-width, separated by 5° [11]. Testing the receptive field of the central of three columnar CT1 compartments, we found a spatial receptive field half-width of 9.6° (Figure 3C). Hence, the receptive field is largely determined by the spatial sensitivity of the input and closely replicates the experimental findings. In order to detect visual movement, local motion detectors must receive input signals that are separated in space and in time. To probe whether CT1 terminals fulfill this requirement, we presented the model cell with a sine grating (Figure 3D). When the stimulus was stationary, we observed that the membrane potential in neighboring terminals changed according to the phase of the grating (Figure 3D, left), further corroborating the results from our receptive field analysis. Once the grating was moved in one direction, voltage responses of individual terminals were modulated robustly at the temporal frequency of the stimulus. Critically for motion detection, phase delays between signals were preserved (Figure 3D, right). This illustrates that CT1 terminals retain information about the spatial as well as the temporal characteristics of the input signal and further demonstrates their usefulness in the motion detection pathway.

Using functional 2-photon calcium imaging and anatomically realistic compartmental modeling, we thus provide strong evidence for an extreme case of electrically isolated sub-compartments in a large-field amacrine cell, which functions as many hundred independent processing units. This has important implications for the potential role of CT1 in motion processing in the visual system of *Drosophila*. Recently, several studies have demonstrated that the computation of direction selectivity in

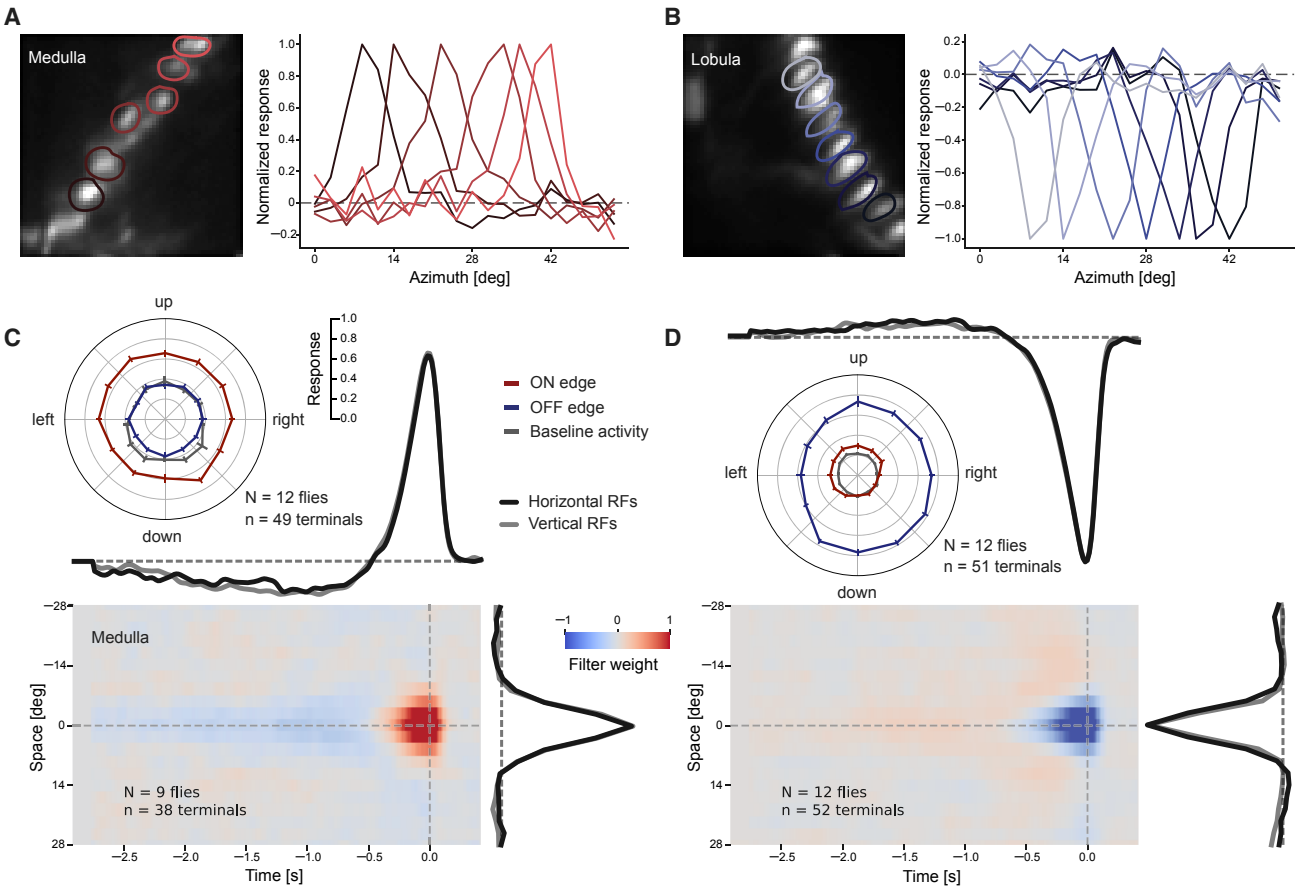

Figure 2. Functional 2-Photon Calcium Imaging in CT1 Terminals

(A and B) Left: average 2-photon image of CT1 terminals in the medulla (A) and the lobula (B). Red and blue circles indicate hand-drawn regions of interest (ROIs). Right: example spatial receptive fields of neighboring CT1 terminals in the medulla (A) and the lobula (B) based on white-noise analysis are shown. Color code corresponds to respective ROIs on the left.

(C and D) Response characteristics of CT1 terminals in the medulla (C) and the lobula (D). Polar plots indicate average responses of CT1 to moving bright (red) and dark (blue) edges in 12 directions (error bars: 68% confidence interval). Grey traces indicate baseline levels. Heatmaps show spatiotemporal receptive fields measured with white noise patterns along the azimuth. Traces on top and to the right indicate cross sections along the temporal and spatial domain, respectively (dashed lines). Grey traces are derived from measurements along the elevation; black traces correspond to receptive fields along the azimuth.

For more detailed receptive field analysis and variability over ROIs, see also Figure S1.

the fly brain is based on both preferred direction enhancement and null direction suppression [14–16]. As a result, presynaptic elements to the elementary motion detectors T4 and T5 must contribute both excitation (on the preferred side) and inhibition (on the null side). Although evidence for inhibitory, columnar inputs to T4 has been shown before [6], the only cell type in the OFF pathway potentially providing null direction suppression is the GABAergic wide-field neuron CT1 [6, 7]. In this study, we demonstrate that CT1 can indeed perform local computations and is therefore a promising candidate for the direction selectivity circuit, whose exact role has to be further investigated in the future.

In our experiments, we measured changes in calcium concentration, whereas in the modeling section, we calculated membrane voltage distributions. Potential discrepancies between these two readouts of neural activity need to be kept in mind [9, 10, 17]. It is possible that the transformation from underlying membrane polarization to voltage-gated calcium dynamics either enhances or reduces compartmentalization between terminals through compressive or expansive channel activation functions. Any model of this transformation would require knowledge of channel properties and distribution that is currently not available. However, a recent study has shown that, if anything, calcium signaling tends to be more compartmentalized than voltage in the fly visual system [17]. Finally, because synaptic output depends on calcium concentration at release sites, the strong compartmentalization we observe in our calcium measurements should be of immediate functional relevance.

In summary, our results show that, in order to ensure an electrical decoupling of the different processes of an amacrine cell in the small brain of the fly, connecting branches have to be long and thin. Additionally, either specific axial resistance has to be unusually high or membrane resistance must be at the low end of the spectrum. This demonstrates that such an extreme case of compartmentalization is at the biophysical limit of neural computation.

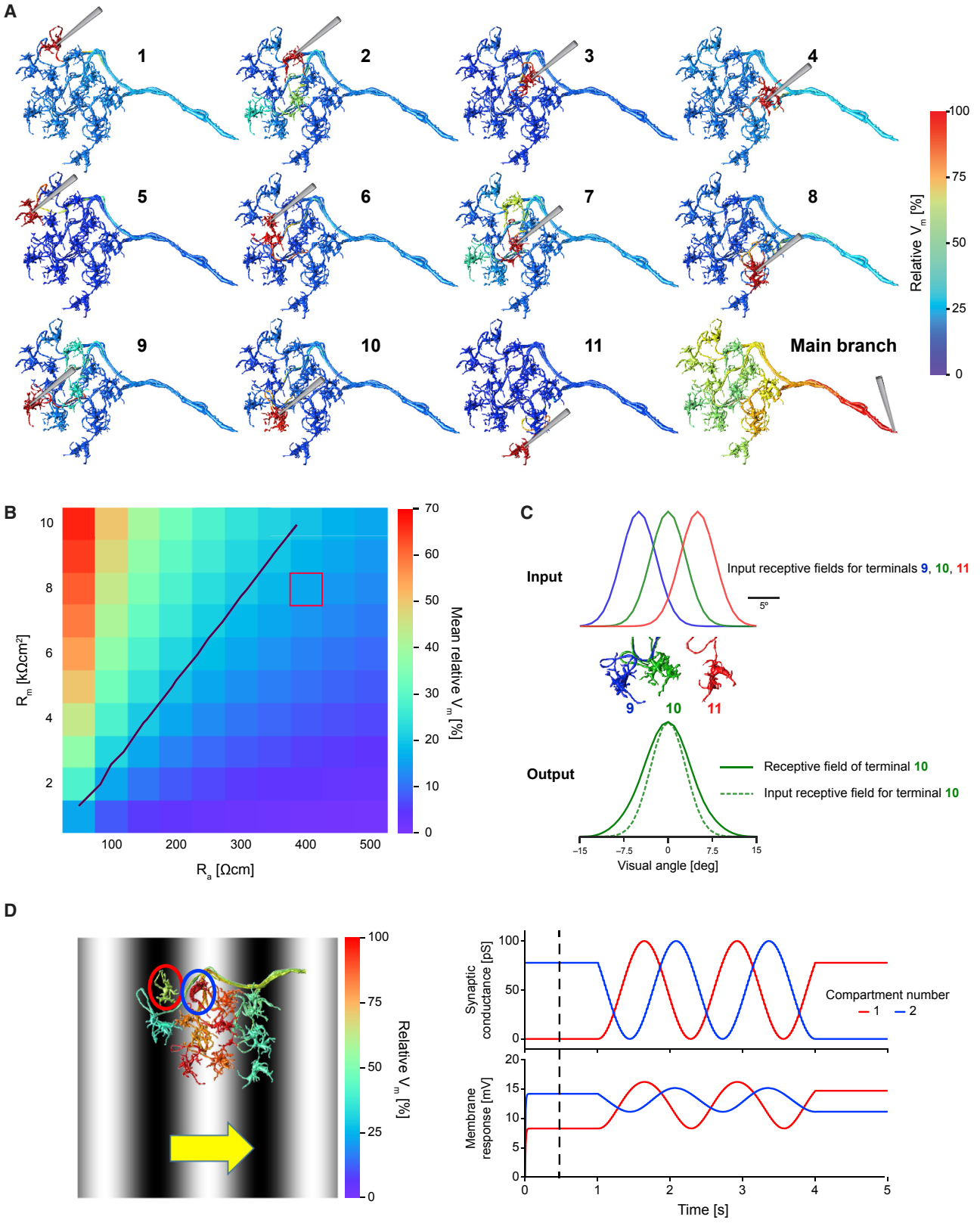

(legend on next page)

STAR★METHODS

Detailed methods are provided in the online version of this paper and include the following:

- KEY RESOURCES TABLE
- CONTACT FOR REAGENT AND RESOURCE SHARING
- EXPERIMENTAL MODEL AND SUBJECT DETAILS
- METHOD DETAILS
  - Immunohistochemistry and confocal imaging
  - Two-photon-microscopy and data acquisition
  - Visual stimulation
  - Modeling
- QUANTIFICATION AND STATISTICAL ANALYSIS
- DATA AND SOFTWARE AVAILABILITY

SUPPLEMENTAL INFORMATION

Supplemental Information can be found online at https://doi.org/10.1016/j.cub.2019.03.070.

ACKNOWLEDGMENTS

We thank A. Leonhardt for help with data analysis and, together with E. Serbe, for carefully reading the manuscript; M. Drews for development and help with visual stimuli and data acquisition; and H. Peng for support with the visualization using Vaa3D. The work was supported by the Max-Planck Society.

AUTHOR CONTRIBUTIONS

M.M. performed and evaluated calcium imaging experiments. A.B. performed all modeling work. A.B. and M.M. jointly designed the study and wrote the manuscript.

DECLARATION OF INTERESTS

The authors declare no competing interests.

Received: January 28, 2019
Revised: March 8, 2019
Accepted: March 28, 2019
Published: April 25, 2019

REFERENCES

1. Euler, T., Detwiler, P.B., and Denk, W. (2002). Directionally selective calcium signals in dendrites of starburst amacrine cells. Nature *418*, 845–852.
2. Grimes, W.N., Zhang, J., Graydon, C.W., Kachar, B., and Diamond, J.S. (2010). Retinal parallel processors: more than 100 independent microcircuits operate within a single interneuron. Neuron *65*, 873–885.
3. Masland, R.H. (2012). The tasks of amacrine cells. Vis. Neurosci. *29*, 3–9.
4. Laurent, G., and Burrows, M. (1989). Intersegmental interneurons can control the gain of reflexes in adjacent segments of the locust by their action on nonspiking local interneurons. J. Neurosci. *9*, 3030–3039.
5. Shinomiya, K., Takemura, S.Y., Rivlin, P.K., Plaza, S.M., Scheffer, L.K., and Meinertzhagen, I.A. (2015). A common evolutionary origin for the ON- and OFF-edge motion detection pathways of the *Drosophila* visual system. Front. Neural Circuits *9*, 33.
6. Takemura, S.Y., Nern, A., Chklovskii, D.B., Scheffer, L.K., Rubin, G.M., and Meinertzhagen, I.A. (2017). The comprehensive connectome of a neural substrate for 'ON' motion detection in *Drosophila*. eLife *6*, e24394.
7. Shinomiya, K., Huang, G., Lu, Z., Parag, T., Xu, C.S., Aniceto, R., Ansari, N., Cheatham, N., Lauchie, S., Neace, E., et al. (2019). Comparisons between the ON- and OFF-edge motion pathways in the *Drosophila* brain. eLife *8*, e40025.
8. Maisak, M.S., Haag, J., Ammer, G., Serbe, E., Meier, M., Leonhardt, A., Schilling, T., Bahl, A., Rubin, G.M., Nern, A., et al. (2013). A directional tuning map of Drosophila elementary motion detectors. Nature *500*, 212–216.
9. Single, S., and Borst, A. (1998). Dendritic integration and its role in computing image velocity. Science *281*, 1848–1850.
10. Haag, J., and Borst, A. (2000). Spatial distribution and characteristics of voltage-gated calcium signals within visual interneurons. J. Neurophysiol. *83*, 1039–1051.
11. Arenz, A., Drews, M.S., Richter, F.G., Ammer, G., and Borst, A. (2017). The temporal tuning of the Drosophila motion detectors is determined by the dynamics of their input elements. Curr. Biol. *27*, 929–944.
12. Cuntz, H., Forstner, F., Schnell, B., Ammer, G., Raghu, S.V., and Borst, A. (2013). Preserving neural function under extreme scaling. PLoS ONE *8*, e71540.
13. Borst, A., and Single, S. (2000). Local current spread in electrically compact neurons of the fly. Neurosci. Lett. *285*, 123–126.
14. Haag, J., Arenz, A., Serbe, E., Gabbiani, F., and Borst, A. (2016). Complementary mechanisms create direction selectivity in the fly. eLife *5*, e17421.
15. Leong, J.C.S., Esch, J.J., Poole, B., Ganguli, S., and Clandinin, T.R. (2016). Direction selectivity in *Drosophila* emerges from preferred-direction enhancement and null-direction suppression. J. Neurosci. *36*, 8078–8092.
16. Haag, J., Mishra, A., and Borst, A. (2017). A common directional tuning mechanism of *Drosophila* motion-sensing neurons in the ON and in the OFF pathway. eLife *6*, e29044.
17. Yang, H.H., St-Pierre, F., Sun, X., Ding, X., Lin, M.Z., and Clandinin, T.R. (2016). Subcellular imaging of voltage and calcium signals reveals neural processing in vivo. Cell *166*, 245–257.
18. Chen, T.W., Wardill, T.J., Sun, Y., Pulver, S.R., Renninger, S.L., Baohan, A., Schreiter, E.R., Kerr, R.A., Orger, M.B., Jayaraman, V., et al. (2013). Ultrasensitive fluorescent proteins for imaging neuronal activity. Nature *499*, 295–300.
19. Schnell, B., Joesch, M., Forstner, F., Raghu, S.V., Otsuna, H., Ito, K., Borst, A., and Reiff, D.F. (2010). Processing of horizontal optic flow in three visual interneurons of the Drosophila brain. J. Neurophysiol. *103*, 1646–1657.
20. Denk, W., Strickler, J.H., and Webb, W.W. (1990). Two-photon laser scanning fluorescence microscopy. Science *248*, 73–76.

Figure 3. Realistic Compartmental Model of CT1

(A) Simulated voltage distribution upon current injection into one of 11 different columnar terminals and the main branch of an anatomical model of CT1 (injection sites indicated by gray electrode; electron-microscopy [EM] data from [7]). Membrane voltage values are normalized to their maximum in the injected compartment (see color bar on the right). Input resistances are comparable for all compartments (about 2GΩ), except for the main branch (about 1GΩ).

(B) Average relative membrane voltage across all neighboring terminals upon current injections in one columnar compartment for a set of realistic membrane parameters (axial resistances R_a and transmembrane resistances R_m). Red square indicates parameter set used for simulations in (A). Black line indicates 20% level.

(C) Spatial receptive field of one CT1 terminal (terminal 10) upon simulated synaptic inputs into three neighboring CT1 terminals (9, 10, and 11).

(D) Stimulation of neighboring CT1 receptive fields with a sine grating (15° spatial wavelength). (Left) Color-coded relative V_m of CT1 at the time point indicated by the dashed line on the right. (Right) Synaptic conductance (top) and membrane response (bottom) of two neighboring terminals over time (1 and 2; highlighted by circles on the left) when stimulated with a moving sinewave grating are shown.

21. Peng, H., Ruan, Z., Long, F., Simpson, J.H., and Myers, E.W. (2010). V3D enables real-time 3D visualization and quantitative analysis of large-scale biological image data sets. Nat. Biotechnol. *28*, 348–353.

22. Peng, H., Bria, A., Zhou, Z., Iannello, G., and Long, F. (2014). Extensible visualization and analysis for multidimensional images using Vaa3D. Nat. Protoc. *9*, 193–208.

23. Peng, H., Tang, J., Xiao, H., Bria, A., Zhou, J., Butler, V., Zhou, Z., Gonzalez-Bellido, P.T., Oh, S.W., Chen, J., et al. (2014). Virtual finger boosts three-dimensional imaging and microsurgery as well as terabyte volume image visualization and analysis. Nat. Commun. *5*, 4342.

24. Jia, H., Rochefort, N.L., Chen, X., and Konnerth, A. (2011). In vivo two-photon imaging of sensory-evoked dendritic calcium signals in cortical neurons. Nat. Protoc. *6*, 28–35.

STAR★METHODS

KEY RESOURCES TABLE

REAGENT or RESOURCE	SOURCE	IDENTIFIER
Antibodies		
Rabbit polyclonal anti-GFP	Acris, OriGene Technologies	Cat#TP401; RRID: AB_10013661
Mouse monoclonal anti-nc82	Developmental Studies Hybridoma Bank (DSHB)	RRID: AB_2314866
Goat polyclonal anti-rabbit Alexa 488	Invitrogen	Cat#A11034; RRID: AB_2576217
Goat polyclonal anti-mouse Alexa 568	Invitrogen	Cat#A11004; RRID: AB_141371
Deposited Data		
Modeled CT1 neuron (.swc file)	[7], this paper	https://github.com/borstlab/ct1_paper
Experimental Models: Organisms/Strains		
D. melanogaster: w^+; R65E11-AD; R20C09-DBD	[6]	N/A
D. melanogaster: w^+; P{20XUAS-IVS-GCaMP6f}attP40; +	Bloomington Drosophila Stock Center	BL 42747
D. melanogaster: w^+; +; PBac{20XUAS-IVS-GCaMP6f}VK00005	Bloomington Drosophila Stock Center	BL 52869
Software and Algorithms		
Model Python Code	This paper	https://github.com/borstlab/ct1_paper

CONTACT FOR REAGENT AND RESOURCE SHARING

Further information and requests for resources and reagents should be directed to and will be fulfilled by the Lead Contact, Matthias Meier (mmeier@neuro.mpg.de).

EXPERIMENTAL MODEL AND SUBJECT DETAILS

Flies (*Drosophila melanogaster*) were raised on standard cornmeal-agar medium with 12hr light/ 12hr dark cycles, 25°C, and 60% humidity. For all experiments we used 1-3 days old female flies of the genotype w+; R65E11-AD/UAS-GCaMP6f; R20C09-DBD/UAS-GCaMP6f [6, 18].

METHOD DETAILS

Immunohistochemistry and confocal imaging

Immunostainings were performed as described in [19] using primary antibodies for GFP to visualize GCaMP expression and the presynaptic marker nC82 as reference background staining. Primary antibodies were used with a concentration of 1:1000 and 1:20 for rabbit-anti-GFP and mouse-anti-nC82, respectively. For visualization the following secondary antibodies were used: goat-anti-rabbit-Alexa 488 and goat-anti-mouse-Alexa 568 (Molecular Probes) with a concentration of 1:500. After the staining procedure the brains were mounted in Slow FadeTM (Invitrogen) and optically sectioned with a confocal microscope (Leica SP5). The image-stacks were subsequently processed for illustration in Fiji.

Two-photon-microscopy and data acquisition

Calcium imaging experiments were performed as previously described in [11]. In brief, flies were cold anesthetized on ice, mounted on a plexi-glass holder and the cuticle on the right hemisphere was removed to gain optical access to the brain. The flies were then placed under a custom built 2-photon laser scanning microscope [20] controlled by the ScanImage 3.8 software (Vidrio Technologies, LLC). Acquisitions were performed at a rate of 15.02 Hz with an image resolution of 64x64 pixels.

Visual stimulation

Visual stimuli were presented to the fly on a custom built arena as described in [11]. In the beginning of every experiment a region of visually responsive CT1-terminals was located using full-field flicker stimuli. Recordings for lobula and medulla terminals were performed separately, except for the directional tuning experiment, where the imaged region contained both neuropils. The first visual

stimulus consisted of moving bright (ON) and dark (OFF) edges of full contrast (max. luminance 276 +- 48 cd/m2) traveling in 12 directions. Each stimulus was repeated three times and the resulting protocol was presented in a randomized fashion.

In the second set of experiments, Gaussian noise stimuli were used to determine the spatiotemporal receptive fields of single CT1 terminals. Azimuth and elevation were tested separately using vertical and horizontal patterns, respectively. For the azimuth the cylindrical arena was partitioned in 64 bars, while in the vertical axis 54 bars were used. Each bar covered approximately 2.8 degrees in visual space and its luminance was modulated at 60 Hz (see [11] for more detailed description). The luminance value of each bar was drawn at each frame from a Gaussian distribution around a mean value of 50 on an 8-bit grayscale display, with a standard deviation of 25%.

Modeling

For illustrations in Figure 1C and visualization of voltage distribution in Figure 3A, we used electron microscopy data from [7] available online (http://emdata.janelia.org/optic-lobe/) processed with Vaa3D (Copyright 2006-2012 Howard Hughes Medical Institute - Janelia Research Campus; 2013-2016 Allen Institute and Howard Hughes Medical Institute - Janelia Research Campus [21–23]).

To build a passive compartmental model of the CT1 cell, separate .swc files from EM reconstructions were first loaded in the Vaa3d software to determine the respective compartment numbers at which the processes touch each other. After that, the separate branches were stitched together resulting in a single .swc file ('BigCT1.swc') with 3749 continuously numbered compartments using a custom written Python code called 'CT1stitcher.py'. In order to ensure that a parent branch had already occurred before a daughter branch could be assigned to be connected to it, this procedure required extensive renumbering of the compartments. The resulting .swc file was then used for compartmental modeling with the software called 'CompModeling.py', again written in Python. Briefly, we first calculated an Adjacency matrix that indicated by a '1' in cell *[i,j]* and cell *[j,i]* if compartment *i* was connected to compartment *j* and held '0's otherwise. In the next step, we calculated from the Adjacency matrix a conductance matrix *M*, based on the x-, y-, and z-coordinates and diameters of each compartment number using specific parameters for the transmembrane resistance R_m, the axial resistance R_a and the specific membrane capacity C_m. If not stated otherwise, we used the following values: $R_m = 8000\ \Omega cm^2$, $R_a = 400\ \Omega cm$ and $C_m = 0.6\ \mu F/cm^2$. Next, the program determined the membrane voltage $V_m[t]$ at each compartment and at each point in time *t* by iteratively solving the matrix equation $M * V_m[t] = R$, with $R = V_m[t-1] * mc / \Delta t + ci[t]$, i.e., the membrane potential at the previous time point $V_m[t-1]$, multiplied by the membrane capacity *mc*, divided by Δt, plus *ci*, the current injected at this time point. If only steady-state was considered, the diagonal of the conductance matrix held no capacitive conductance and the right-hand side of the equation simplified to the current vector. If synaptic input was simulated, the synaptic current vector was added to the diagonal of the conductance matrix and, multiplied by the driving force of the current, to the right-hand side of the equation as well. To visualize the membrane voltage distribution across the CT1 cell (Figure 3A), the membrane potential was normalized to its maximum value and stored as integer values between 20 and 20+255 within the second column of the .swc file. This file was then read by the Vaa3d software which led to the images displayed in Figure 3A.

QUANTIFICATION AND STATISTICAL ANALYSIS

All acquired data were analyzed with custom written software in Python 2.7 (see [11]). Image registration was performed automatically using vertical and horizontal translations.

Relative fluorescence changes (ΔF/F) from raw calcium traces were obtained by adapting an automatic baseline detection algorithm [24]. Briefly, raw data were first smoothed with a Gaussian window (full-width at half maximum, FWHM = 1 s). Then, minima within a 90 s long sliding window were extracted and the resulting trace smoothed with a Gaussian window (FWHM = 4 min). The result was used as a dynamic baseline F0 and ΔF/F values were computed as ΔF/F = (F-F0)/F0. Regions of interest (ROI) were drawn manually, covering single CT1-terminals in both lobula and medulla. For each ROI the signal was spatially averaged to create a ΔF/F time trace. For the directional tuning experiment, all resulting traces were band-pass filtered (tau_{hp}: 100ms, tau_{lp}: 500ms) and subsequently normalized to the maximum response per acquisition and ROI. The response maxima were extracted and averaged over ROIs and flies. Baseline levels were determined by taking the maximum in the two seconds before each visual stimulus presentation. Spatiotemporal receptive fields were determined through reverse-correlation of the calcium responses to the white-noise stimulus for each ROI (see [11]). The resulting receptive fields were normalized in z-score and only ROIs with z-scores above 9 standard deviations from the mean were used for further analysis. Receptive fields close to the borders of the stimulus arena (less than 28 degrees) were excluded. For the heatmap representation in Figure 2, all horizontal RFs were peak aligned and averaged for medulla and lobula separately. Spatial traces were extracted through a cross-section through the peak along the spatial domain. The full-width at half maximum was estimated by fitting a Gaussian function to the average spatial receptive field (R^2 above 0.98 for all conditions). Temporal traces represent a cross-section through 0 degrees in azimuth and elevation, respectively.

DATA AND SOFTWARE AVAILABILITY

Python programs used for the compartmental model as well as the .swc file containing the model-cell are available at https://doi.org/10.5281/zenodo.2636606.

Current Biology, Volume *29*

Supplemental Information

Extreme Compartmentalization in a *Drosophila* Amacrine Cell

Matthias Meier and Alexander Borst

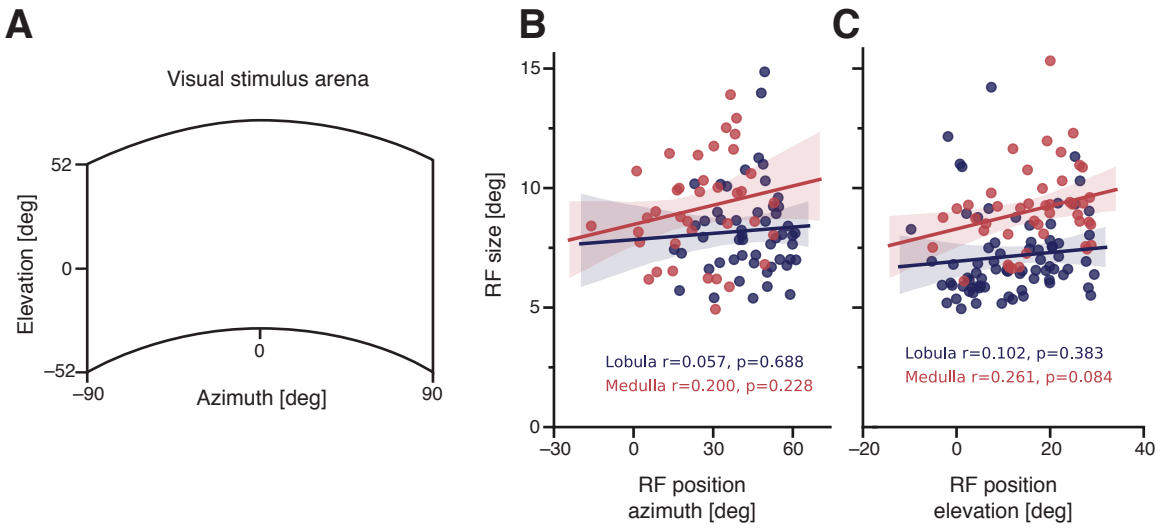

Figure S1 Receptive field sizes and distributions, Related to Figure 2 (**A**) Schematic depicting the visual stimulation device (arena), covering approximately 180° in azimuth and 104° in elevation. (**B**) Receptive field size (FWHM, estimated by Gaussian fits) depending on the receptive field location for horizontal bar-noise experiments. Each point corresponds to one ROI in either the medulla (red) or the lobula (blue). The lines depict regression model fits between the receptive field size and position along the azimuth. Pearson's correlation coefficient (r) and 2-tailed p-values (p) are indicated for both lobula and medulla. (**C**) Receptive field correlation plots for vertical bar noise experiments (same as in B). Error shades indicated 95% confidence inter-